Int. J. Multiphase Flow, Vol. 2, pp. 153–169. Pergamon/Elsevier, 1975. Printed in Great Britain

LAMINAR JET CONTRACTION AND VELOCITY DISTRIBUTION IN IMMISCIBLE LIQUID–LIQUID SYSTEMS

H. Yu† and G. F. Scheele
School of Chemical Engineering, Cornell University, Ithaca, NY 14850, U.S.A.

(*Received* 12 *August* 1974)

Abstract—The flow behavior of a Newtonian liquid jet injected vertically into an immiscible Newtonian liquid phase is analyzed. Boundary-layer type approximations are used to simplify the general equations, and an approximate momentum-integral type numerical solution is obtained. This solution predicts the velocity distribution in each phase and the jet radius. The effects on jet behavior of the five dimensionless groups needed to characterize the gravitational, interfacial tension and viscous forces are shown. In particular the importance of the continuous phase viscosity is demonstrated. Experimental measurements of jet radius confirm the essential features of the analysis and illustrate the shortcomings of the approximate solution.

INTRODUCTION

One important technique for creating the large interfacial area required for liquid–liquid extraction and direct contact heat exchange is the injection of one liquid through a nozzle or orifice into a second immiscible liquid. At sufficiently large injection velocities, the formation of discrete drops results from laminar jet breakup caused by the amplification of initially small disturbances to which the jet is inherently unstable.

Meister & Scheele (1969b) have coupled stability theory with the requirement that the disturbances travel at the same velocity as the jet surface to obtain an equation for predicting the size of drops formed from a Newtonian jet injected into a second Newtonian liquid. The equation requires knowledge of the jet radius, the surface velocity, and the disturbance wave number which in turn depends on the velocity distribution in the jet. Improved prediction of these variables is necessary if drop sizes are to be calculated with reasonable accuracy.

Several approximate solutions exist for prediction of jet velocity distributions in liquid–liquid systems. The steady state distribution obtained by Garner *et al.* (1959) by neglecting inertial terms in the equations of motion is not applicable since breakup normally occurs long before steady state is attained. Vandegrift (1963) assumed a form for the velocity distribution in each phase and evaluated the undetermined coefficients from boundary conditions. The major objection to this analysis is that it predicts jet expansion in many cases where contraction is observed experimentally, a consequence primarily of the choice and approximate nature of some of the boundary conditions. Meister & Scheele (1969a) modified Vandegrift's approach by superimposing the jet radius obtained from the simplified dispersed phase momentum balance of Shiffler (1965) onto the velocity profiles obtained from a consideration of viscous forces. The results show distinct improvement over Vandegrift's predictions for jet radius and also show reasonable agreement with very limited interfacial velocity data. However, there are several unsatisfactory features of the analysis. For example, viscous forces are neglected in predicting the jet radius, and no attempt is made to have the continuous phase satisfy continuity or the equations of motion.

Although no completely satisfactory analysis of jet behavior presently exists for liquid–liquid systems, an excellent analysis of the fluid mechanics of a laminar liquid jet in a gaseous continuous phase has been presented by Duda & Vrentas (1967). This case is simpler than the liquid–liquid one because the continuous phase can be neglected, but it still presents formidable mathematical difficulties. Duda & Vrentas used a novel coordinate system to overcome

*Present address: Aluminum Company of America Alcoa Center, PA 15069, U.S.A.

problems associated with the free boundary. They present the elliptic partial differential equations describing jet behavior and obtain numerical and approximate analytical solutions valid for large Reynolds numbers which show excellent agreement with experimental data. At high Reynolds numbers only two dimensionless groups, the Weber number and the ratio of the Reynolds and Froude numbers, are needed to define jet behavior.

The results of Duda & Vrentas are not directly applicable to liquid–liquid systems because they do not include the effects of continuous phase density and viscosity on jet behavior. The buoyant effect plays a significant role in determining jet contraction, while the viscous effect is important in determining the jet velocity distribution. Buoyancy, which can be readily incorporated into the gravitational force term of the dispersed phase equation of motion through modification of the interfacial boundary condition for the pressure differential between dispersed and continuous phases, does not complicate the analysis of Duda & Vrentas. However, a viscous continuous phase significantly increases the complexity, since simultaneous solution of the equations of motion for both liquid phases becomes necessary.

The present paper uses the dispersed phase analysis of Duda & Vrentas as a starting point for the formulation of the equations and boundary conditions necessary to predict laminar jet behavior in immiscible Newtonian liquid–liquid systems. The complexity of the resulting equations makes any exact solution impractical. Instead, an approximate numerical solution is obtained which shows not only the effects of the various physical parameters but also their relative importance.

FORMULATION OF EQUATIONS

Consider the steady laminar injection of an incompressible Newtonian liquid through a long vertical nozzle of circular cross section into a second immiscible and incompressible Newtonian liquid. Assume that the nozzle tip is surrounded by a circular flat plate of infinite radial extent, which simplifies the continuous phase boundary conditions. A diagram of the model geometry is shown in figure 1. The nozzle is sufficiently long that a fully developed parabolic velocity profile exists at the nozzle exit. The flow system is isothermal, and the phases are mutually saturated so that there is no interphase mass transfer. Symmetry is assumed in the azimuthal direction and the velocity in this direction is everywhere set equal to zero. In order to determine the flow characteristics of the jet, the continuity and motion equations have to be formulated for both phases and solved simultaneously. The solution will be valid only in the initial disturbance-free portion of the jet. In the analysis that follows all position coordinates and velocities are nondimensionalized using the nozzle radius R_0 and the jet average axial velocity U_a within the nozzle.

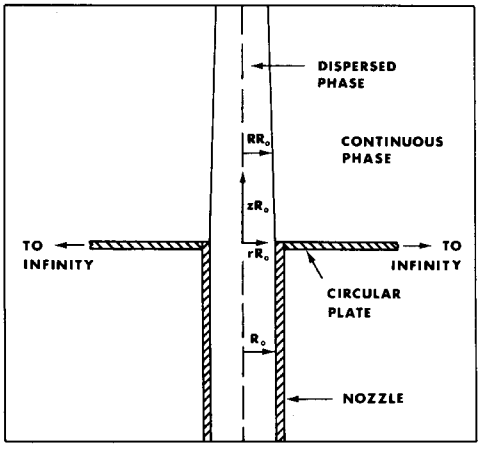

Figure 1. Geometry of the theoretical model.

Dispersed phase

In order to overcome the mathematical difficulties associated with the free jet boundary, it is convenient to adopt the nonorthogonal Protean coordinate system presented by Duda & Vrentas (1967) for analyzing jet flow in an inviscid continuous fluid phase. The significant feature of this coordinate system is that one of the coordinate lines is a streamline, so that the surface of the jet is uniquely defined by the dimensionless stream function $\Psi = 1/2$. The Jacobian of transformation relating the dimensionless Protean coordinates $\bar{x}^1 = \Psi$, $\bar{x}^2 = \theta$, $\bar{x}^3 = \xi$ to the dimensionless cylindrical coordinates $x^1 = r$, $x^2 = \theta$, $x^3 = z$ can be written as

$$\left|\frac{\partial \bar{x}^i}{\partial x^j}\right| = \begin{vmatrix} rv^3 & 0 & -rv^1 \\ 0 & 1 & 0 \\ 0 & 0 & 1 \end{vmatrix} \qquad [1]$$

Additional details of the coordinate system are given by Duda & Vrentas (1967) and Yu (1971).

The one change from the coordinate system used by Duda and Vrentas is the direction of ξ, which is taken opposite the direction of gravity so that the equations as written are valid for injection vertically upward.

Duda & Vrentas present the dimensionless differential equations which are obtained from the equations of motion in the ξ and Ψ directions. They show, by using an order of magnitude analysis, that for nozzle Reynolds numbers larger than about 200 the equations are significantly simplified, reducing to

$$U\frac{\partial U}{\partial \xi} = -\frac{1}{2N_{Fr}} - \frac{1}{\rho U_a^2}\frac{\partial P}{\partial \xi} + \frac{2}{N_{Re}}\left[2U\frac{\partial U}{\partial \Psi} + r^2 U\left(\frac{\partial U}{\partial \Psi}\right)^2 + r^2U^2\frac{\partial^2 U}{\partial \Psi^2}\right] \qquad [2]$$

$$\frac{\partial P}{\partial \Psi} = 0, \qquad [3]$$

where U is the dimensionless axial velocity. The Froude number N_{Fr} is $U_a^2/2\,R_0 g$ and the dispersed phase Reynolds number N_{Re} is $2R_0\,\rho U_a/\mu$, where ρ and μ are the dispersed phase density and viscosity. Equation [2] differs from Duda & Vrentas' equation [79] only in the sign change on the Froude number term which results from inversion of the coordinate system. The approximation given by [3] makes it possible to relate the pressure distribution $P(\xi)$ directly to the continuous phase pressure distribution by using an interfacial boundary condition.

Two additional dispersed phase relationships, which can be obtained from [1], are

$$\frac{\partial r}{\partial \Psi} = \frac{1}{rU}, \qquad [4]$$

which relates the radial coordinate r to the Protean coordinate Ψ, and

$$\frac{\partial r}{\partial \xi} = \frac{V}{U}, \qquad [5]$$

which is needed to calculate the dimensionless radial velocity V. Equations [4] and [5] are identical to Duda & Vrentas' equations [35] and [36].

Continuous phase

The presence of a liquid continuous phase significantly complicates the analysis. For a gaseous continuous phase Duda & Vrentas were able to assume an inviscid fluid of constant pressure, but such simplifications are not possible for a liquid.

It is more convenient to use the cylindrical coordinate system for the continuous phase

equations, because in Protean coordinates the continuous phase streamlines become essentially perpendicular to the nozzle in the region near the nozzle tip. The superscript ° is used to distinguish continuous phase from dispersed phase variables.

For an axially symmetrical flow the dimensionless continuity equation is

$$\frac{1}{r}\frac{\partial}{\partial r}(rV^\circ)+\frac{\partial U^\circ}{\partial z}=0. \qquad [6]$$

The z-component of the equation of motion is

$$V^\circ\frac{\partial U^\circ}{\partial r}+U^\circ\frac{\partial U^\circ}{\partial z}=-\frac{1}{\rho^\circ U_a^2}\frac{\partial P^\circ}{\partial z}+\frac{2}{N_{Re^\circ}}\left[\frac{1}{r}\frac{\partial}{\partial r}\left(r\frac{\partial U^\circ}{\partial r}\right)+\frac{\partial^2 U^\circ}{\partial z^2}\right]-\frac{gR_0}{U_a^2}, \qquad [7]$$

and the r-component is

$$V^\circ\frac{\partial V^\circ}{\partial r}+U^\circ\frac{\partial V^\circ}{\partial z}=-\frac{1}{\rho^\circ U_a^2}\frac{\partial P^\circ}{\partial r}+\frac{2}{N_{Re^\circ}}\left\{\frac{\partial}{\partial r}\left[\frac{1}{r}\frac{\partial}{\partial r}(rV^\circ)\right]+\frac{\partial^2 V^\circ}{\partial z^2}\right\}, \qquad [8]$$

where the continuous phase Reynolds number N_{Re° is defined as

$$N_{Re^\circ}=2R_0U_a\rho^\circ/\mu^\circ. \qquad [9]$$

To simplify [7] and [8] a boundary layer analysis similar to that used by Sakiadis (1961) and by Vasudevan & Middleman (1970) to predict axisymmetric boundary layer growth in the direction of motion on a continuous cylindrical solid surface is employed. The previous results cannot be applied directly to laminar liquid jets because contraction and the relaxation of the interfacial velocity were not considered.

For continuous phase Reynolds numbers greater than about 100, Yu (1971) has shown from an order of magnitude analysis that within the boundary layer [7] and [8] are simplified to

$$V^\circ\frac{\partial U^\circ}{\partial r}+U^\circ\frac{\partial U^\circ}{\partial z}=-\frac{1}{\rho^\circ U_a^2}\frac{\partial P^\circ}{\partial z}+\frac{2}{N_{Re^\circ}}\left[\frac{1}{r}\frac{\partial}{\partial r}\left(r\frac{\partial U^\circ}{\partial r}\right)\right]-\frac{gR_0}{U_a^2}, \qquad [10]$$

and

$$\frac{\partial P^\circ}{\partial r}=0. \qquad [11]$$

P° can thus be evaluated from the z component of the equation of motion external to the boundary layer, which reduces to

$$\frac{\partial P^\circ}{\partial z}=-\rho^\circ gR_0. \qquad [12]$$

Substitution of [12] into [10] gives finally

$$V^\circ\frac{\partial U^\circ}{\partial r}+U^\circ\frac{\partial U^\circ}{\partial z}=\frac{2}{N_{Re^\circ}}\left[\frac{1}{r}\frac{\partial}{\partial r}\left(r\frac{\partial U^\circ}{\partial r}\right)\right]. \qquad [13]$$

It should be noted that in the region near the nozzle tip the continuous phase streamlines are essentially perpendicular to the jet. The flow conditions near the nozzle are thus different from

those treated in most boundary layer analyses. Specifically, the radial velocity component may be sufficiently large that [11] is not satisfied.

Interface

The interfacial equations of motion used by Duda & Vrentas require modification since the viscous stresses associated with the continuous phase must be incorporated into the equations.

For Newtonian fluids the Ψ component of the equation of motion can be written in dimensionless form as

$$\frac{P-P^\circ}{\rho U_a^2}+\frac{4(1-\mu^\circ/\mu)}{N_{Re}}\left(\frac{V}{r}+\frac{U^2}{q^2}\frac{\partial U}{\partial \xi}+\frac{UV}{q^2}\frac{\partial V}{\partial \xi}\right)+\frac{2}{N_{We}}\left(\frac{U^2}{q^3}\frac{\partial V}{\partial \xi}-\frac{UV}{q^3}\frac{\partial U}{\partial \xi}-\frac{U}{rq}\right)=0, \qquad [14]$$

where the Weber number N_{We} is $2R_0 U_a^2 \rho/\sigma$ and σ is the interfacial tension. Similarly, the ξ and Ψ components can be combined, eliminating the pressure term, to obtain the dimensionless equation

$$\mu\left(\frac{rq^2}{V}\frac{\partial U}{\partial \Psi}\right)-\mu^\circ\left(\frac{rq^2}{V}\frac{\partial U^\circ}{\partial \Psi}\right)+(\mu-\mu^\circ)\left(-\frac{\partial U}{\partial \xi}-\frac{V}{r}+\frac{U}{V}\frac{\partial V}{\partial \xi}-\frac{2U^2}{q^2}\frac{\partial U}{\partial \xi}-\frac{2UV}{q^2}\frac{\partial V}{\partial \xi}\right)=0, \qquad [15]$$

where

$$q=(U^2+V^2)^{1/2}. \qquad [16]$$

For an inviscid continuous phase $\mu^\circ=0$, and [14] and [15] reduce to equations [73] and [72] presented by Duda & Vrentas (1967).

For large dispersed phase Reynolds numbers, an order of magnitude analysis reduces [15] to

$$\mu\frac{\partial U}{\partial \Psi}=\mu^\circ\frac{\partial U^\circ}{\partial \Psi} \quad \text{at} \quad \Psi=1/2, \qquad [17]$$

and [14] to

$$\frac{P-P^\circ}{\rho U_a^2}=\frac{2}{RN_{We}}-\frac{4(1-\mu^\circ/\mu)}{N_{Re}}\frac{\partial U}{\partial \xi} \quad \text{at} \quad \Psi=1/2, \qquad [18]$$

where R is the dimensionless jet radius. In order to simplify the computations, the analysis in this study is limited to cases where $N_{Re}/(1-\mu^\circ/\mu)$ is sufficiently large that [18] reduces to

$$\frac{P-P^\circ}{\rho U_a^2}=\frac{2}{RN_{We}}. \qquad [19]$$

Shiffler (1965) incorrectly used the expression $(P-P^\circ)/\rho U_a^2=4/RN_{We}$ in deriving his equation for jet radius, and Meister & Scheele (1969a) incorporated the resulting incorrect equation into their velocity profile analysis.

Equation [11] shows that the radial pressure gradient within the boundary layer is negligible. It follows directly that within the boundary layer $\partial P^\circ/\partial \xi|_\Psi=\partial P^\circ/\partial z|_r$, except perhaps in the region close to the nozzle tip where [11] may not be valid. Equations [19] and [12] can then be used to eliminate the pressure from [2], giving

$$U\frac{\partial U}{\partial \xi}=\frac{1}{2N_{Fr}}\left(\frac{\rho^\circ}{\rho}-1\right)+\frac{1}{R^3N_{We}}\frac{dR^2}{d\xi}+\frac{2}{N_{Re}}\left[2U\frac{\partial U}{\partial \Psi}+r^2U\left(\frac{\partial U}{\partial \Psi}\right)^2+r^2U^2\frac{\partial^2 U}{\partial \Psi^2}\right]. \qquad [20]$$

Equation [20] differs from the dispersed phase momentum balance obtained by Duda & Vrentas

for a gaseous continuous phase only in the addition of the factor $[(\rho^\circ/\rho) - 1]$ to the gravity force term. For injection vertically downward the appropriate factor is $[1 - (\rho^\circ/\rho)]$.

It is convenient for computational purposes to introduce a new dimensionless axial variable

$$\zeta = \xi/N_{Re} = z/N_{Re}. \qquad [21]$$

Equation [1] shows the equivalence of ξ and z. Equation [20] then becomes

$$U\frac{\partial U}{\partial \zeta} = \frac{N_j}{2} + \frac{1}{R^3 N_{We}}\frac{dR^2}{d\zeta} + 2\left[2U\frac{\partial U}{\partial \Psi} + r^2 U\left(\frac{\partial U}{\partial \Psi}\right)^2 + r^2 U^2\frac{\partial^2 U}{\partial \Psi^2}\right], \qquad [22]$$

where

$$N_j = N_{Re}\left(\frac{\rho^\circ}{\rho} - 1\right)\Big/ N_{Fr}. \qquad [23]$$

N_j is a generalized buoyancy parameter consistent with the definition $N_j = N_{Re}/N_{Fr}$ used by Duda & Vrentas for injection vertically downward into a zero-density continuous phase.

If the viscous terms are neglected and the velocity profile is assumed flat, [20] can be integrated to obtain the relationship between jet radius and distance from the nozzle first presented by Addison & Elliott (1949, 1950) for liquid–gas systems. Shiffler extended the analysis to liquid–liquid systems to obtain

$$\zeta = \frac{1}{N_j}\left[\left(\frac{1}{R^4} - 1\right) + \frac{4}{N_{We}}\left(\frac{1}{R} - 1\right)\right]. \qquad [24]$$

Using the dimensionless axial coordinate defined by [21], [5], [6] and [13] become

$$\frac{1}{N_{Re}}\frac{\partial r}{\partial \zeta} = \frac{V}{U}, \qquad [25]$$

$$\frac{1}{r}\frac{\partial}{\partial r}(rV^\circ) + \frac{1}{N_{Re}}\frac{\partial U^\circ}{\partial \zeta} = 0, \qquad [26]$$

$$V^\circ\frac{\partial U^\circ}{\partial r} + \frac{U^\circ}{N_{Re}}\frac{\partial U^\circ}{\partial \zeta} = \frac{2}{N_{Re^\circ}}\left[\frac{1}{r}\frac{\partial}{\partial r}\left(r\frac{\partial U^\circ}{\partial r}\right)\right]. \qquad [27]$$

Note that the partial derivatives with respect to ζ are evaluated at constant Ψ in [22] and [25] and at constant r in [26] and [27].

Equations [4], [22], [25], [26] and [27] form the set of simultaneous non-linear differential equations needed to obtain the dispersed and continuous phase velocity distributions and the jet radius. In principle a finite difference solution can be obtained, as Duda and Vrentas showed for the case where the continuous phase can be neglected. However, consideration of the continuous phase made such calculations so lengthy that they were considered impractical for the present study.

APPROXIMATE SOLUTION

To reduce computation time, an integral approach paralleling the momentum integral method for boundary layer flows is adopted. Velocity distributions containing undetermined coefficients which are functions only of axial position are postulated for both phases. This reduces the set of partial differential equations to ordinary differential equations with ζ the independent variable.

The coefficients are evaluated by making the distributions satisfy the initial and boundary conditions, as well as integrated continuity and momentum equations.

Assumed velocity distributions

It is assumed that the dispersed phase axial velocity distribution can be approximated by

$$U = U_c\sqrt{(1 - B\Psi)}, \qquad [28]$$

where U_c, the center-line velocity, and B are functions only of ζ. Equation [28] is the simplest distribution consistent with the initial parabolic profile existing at the nozzle exit, for which $U_c = 2$ and $B = 2$. It is also consistent with the steady-state parabolic distribution obtained by Garner *et al.* (1959) for an infinitely long jet. However, it predicts that for an inviscid continuous phase $U = U_c$ for all $\zeta > 0$, which is inconsistent with the more rigorous results of Duda and Vrentas which show that the profile does not relax instantaneously.

When [28] is substituted into [4] and the result integrated, the relationship between r and Ψ within the jet becomes

$$r^2 = \frac{4}{U_c B}[1 - \sqrt{(1 - B\Psi)}], \qquad [29]$$

so that the jet radius is given by

$$R^2 = \frac{4}{U_c B}[1 - \sqrt{(1 - B/2)}]. \qquad [30]$$

The radial velocity distribution within the jet can also be expressed in terms of U_c and B by substituting [28] and [29] into [25]:

$$V = \frac{1}{N_{Re}}\left[\frac{(1 - B\Psi)U_c}{B[1 - \sqrt{(1 - B\Psi)}]}\right]^{1/2}\left[\left(\frac{\Psi/2}{\sqrt{(1 - B\Psi)}} + \frac{\sqrt{(1 - B\Psi)} - 1}{B}\right)\frac{dB}{d\zeta} + \left(\frac{\sqrt{(1 - B\Psi)} - 1}{U_c}\right)\frac{dU_c}{d\zeta}\right]. \qquad [31]$$

Since [26] and [27] are coupled, distributions are assumed for both continuous phase velocity components,

$$U^\circ = (A + Cr^2)\ln[r/(R + \delta)], \qquad [32]$$

$$V^\circ = (E + Fr^2)\ln[r/(R + \delta)], \qquad [33]$$

where δ, the dimensionless thickness of the boundary layer as measured from the jet surface, and the coefficients A, C, E and F are functions only of ζ. Equations [32] and [33] satisfy the condition that the velocities become zero at the edge of the boundary layer $r = R + \delta$.

Method of solution

The assumed velocity distributions contain seven undetermined coefficients, U_c, δ, A, B, C, E and F. Four boundary conditions and three integral equations are used to obtain the necessary relationships for determining the coefficients.

The first two boundary conditions are continuity of axial and radial velocities at the interface, namely $U = U^\circ$ and $V = V^\circ$ at $r = R$.

The third condition is interfacial continuity of shear stress approximated by [17], and the final boundary condition is $\partial U^\circ/\partial r = 0$ at the edge of the boundary layer $r = R + \delta$.

The integral equations are the dispersed phase equation of motion, obtained by integrating

[22] from $\Psi = 0$ to $\Psi = 1/2$, and the continuous phase continuity and motion equations, obtained by integrating [26] and [27], respectively, from $r = R$ to $r = R + \delta$.

Since the calculation scheme involves a marching procedure in the axial direction starting at the nozzle exit, initial values of the undetermined coefficients are required. For a fully developed parabolic velocity profile exiting from the nozzle, $U_c = 2$ and $B = 2$. For the continuous phase, the injection geometry requires that U° and $V^\circ = 0$ at $\zeta = 0$ for all $r \geq R$. Thus $A = C = E = F = 0$. Finally, by definition the boundary layer thickness $\delta = 0$. It cannot be emphasized too strongly that these initial parameter values are specific to the present study.

The four algebraic equations obtained from the boundary conditions and the three ordinary differential equations obtained from the integral relationships are presented by Yu (1971). A numerical solution is necessary because of the non-linearity of the equations. The differential equations were converted to finite difference form using a backward difference form to approximate derivatives. The set of simultaneous non-linear algebraic equations was then solved using a computational scheme developed by Brown & Samuel (1967). Solution details, including a computer program, are also presented by Yu. Computer time on an IBM 360–65 was about 1 minute per system.

DISCUSSION OF NUMERICAL RESULTS

The analysis shows that the dimensionless velocity distributions and jet radius are functions of the axial distance ζ from the nozzle and five dimensionless groups. Two of these, the buoyancy parameter N_j and the Weber number N_{We}, are sufficient to characterize a jet in an inviscid medium. Three additional dimensionless groups, the dispersed and continuous phase Reynolds numbers N_{Re} and N_{Re° and the viscosity ratio μ/μ°, are needed when the continuous phase viscosity is not negligible.

Numerical studies

Numerical solutions were obtained for ten jet flows. The dimensionless parameters characterizing these flows are summarized in table 1. Also tabulated are two additional dimensionless groups, the density ratio ρ°/ρ and the Froude number N_{Fr}, which are uniquely determined by the specified dimensionless numbers.

Case 1 is the base case, selected to have the same N_j and N_{We} values as the vertical jet calculated by Duda and Vrentas. A viscosity ratio of 1·0 and a density ratio of 2·0 were selected as values typical of many liquid–liquid systems.

The other cases were selected to provide a reasonable variation in each of the five dimensionless groups, subject to the constraint that both Reynolds numbers be sufficiently large to justify the order-of-magnitude simplifications made in the equations of motion. The jet Reynolds number was further restricted to laminar flow values. Emphasis was placed on using values characteristic of real injection systems.

Table 1. Summary of cases analyzed

Case	N_j	N_{We}	N_{Re}	N_{Re°	μ/μ°	ρ°/ρ	N_{Fr}	$d\zeta$
1	128·5	5·4	835	1670	1·0	2·0	6·5	0·0005
2	†	54·0	—	—	—	—	—	0·0005
3	—	0·54	—	—	—	—	—	0·001
4	—	—	1653	—	—	1·01	0·1286	0·0005
5	—	—	165·3	—	—	10·1	11·70	0·003
6	—	—	—	4217	—	5·05	26·3	0·003
7	—	—	—	843	—	1·01	0·065	0·0005
8	—	—	—	—	1·98	1·01	0·065	0·001
9	—	—	—	—	0·198	10·1	59·13	0·003
10	12·85	—	—	—	—	—	65	0·002

†Where not indicated otherwise, parameter values are those of base Case 1.

Table 1 also shows the axial step size $d\zeta$ used in the numerical computations. Step sizes greater than 0.0005 were used only when numerical instabilities were encountered. The effect of step size on calculated results was determined for case 8 by using $d\zeta$ values of 0.001 and 0.003. The effect was greatest near the nozzle. For example, at $\zeta = 0.006$ the interfacial axial velocity increased approximately 5% as the step size was reduced 3-fold, while at $\zeta = 0.027$ the increase was only about 1%. At both axial locations a 3-fold reduction in step size increased the center-line velocity less than 0.3% and reduced the jet radius less than 0.7%. This agreement was considered satisfactory for the present study.

The numerical results are summarized in figures 2–12.

Jet relaxation and momentum change

The effect of the dimensionless parameters can best be explained by first considering the two factors which determine jet behavior, namely the relaxation of the initially parabolic profile and the change in jet momentum produced by the surface and body forces acting on the jet.

When a jet issues from a nozzle, momentum exchange with the core of the jet causes acceleration of the surface fluid. The rate of momentum exchange and hence velocity profile relaxation is greatest near the nozzle where velocity gradients are largest. In the limit that no forces act on the jet, conservation of momentum requires that the radius of a jet with an initially parabolic velocity distribution satisfy the equation

$$R^2 = 3\,k_1/4, \qquad [34]$$

where k_1 is the ratio of jet momentum to the momentum associated with a plug flow jet of equivalent radius. Since k_1 is a function of the jet velocity distribution, decreasing from its initial value of 4/3 as the profile relaxes, jet contraction accompanies profile relaxation. The asymptotic minimum radius predicted by [34] for a fully relaxed jet is $R = 0.866$, a value which should closely approximate the final radius of a high Weber number jet injected horizontally into an essentially inviscid gas phase.

The change in jet momentum caused by forces acting on the jet also affects jet behavior. Modification of [34] to incorporate a changing jet momentum yields the expression

$$R^2 = 3\,k_1/4\,k_2, \qquad [35]$$

where k_2 is the ratio of downstream to initial momentum. Equation [35] shows that an increase in

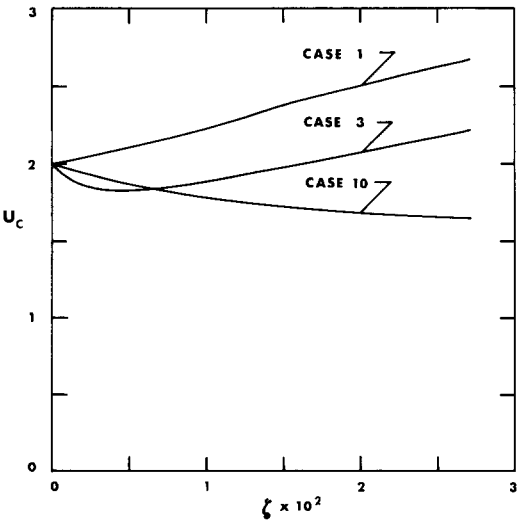

Figure 2. Dependence of jet centerline velocity on axial length.

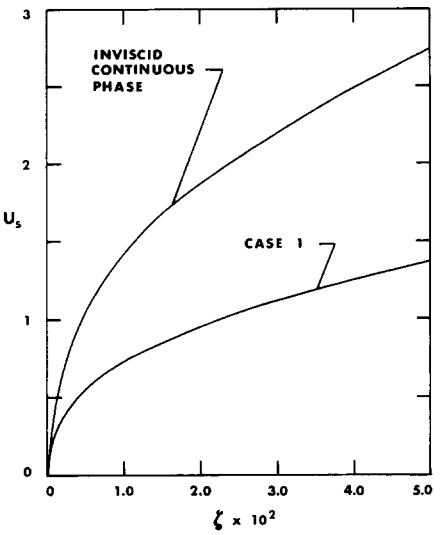

Figure 3. Effect of viscous continuous phase on jet surface velocity for $N_j = 128.5$, $N_{We} = 5.4$.

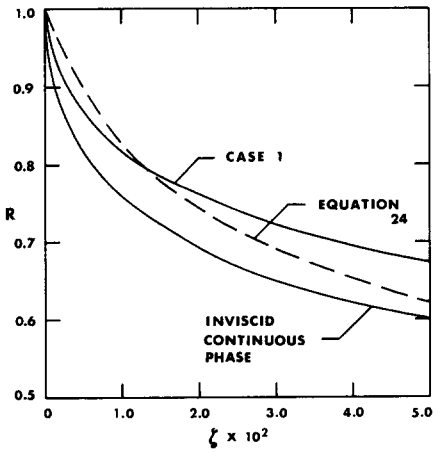

Figure 4. Effect of viscous continuous phase on jet radius for $N_j = 128.5$, $N_{We} = 5.4$.

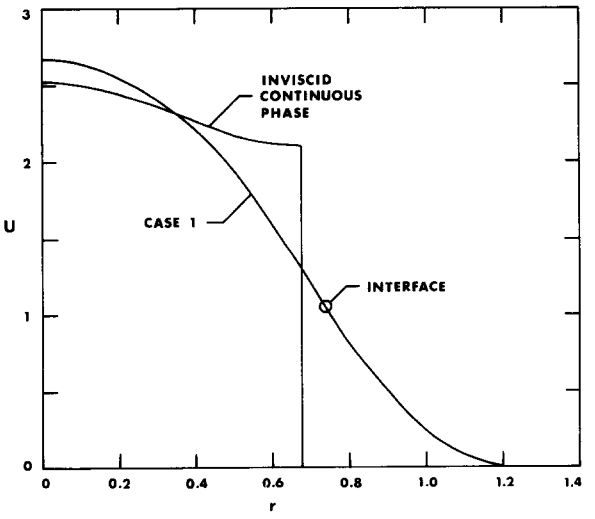

Figure 5. Effect of viscous continuous phase on jet velocity distribution for $N_j = 128.5$, $N_{We} = 5.4$.

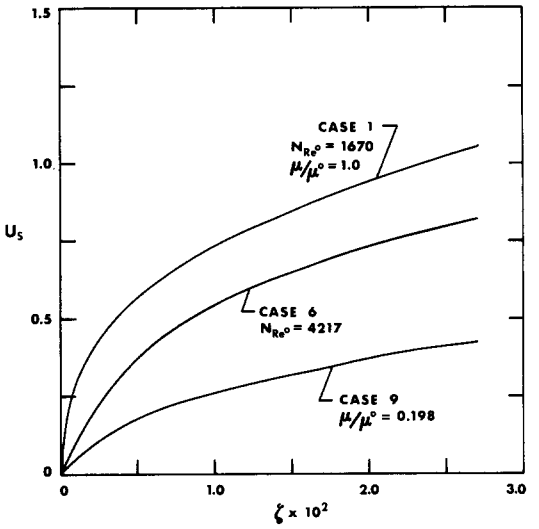

Figure 6. Effects of N_{Re}° and μ/μ° on jet surface velocity for $N_j = 128.5$, $N_{We} = 5.4$, $N_{Re} = 835$.

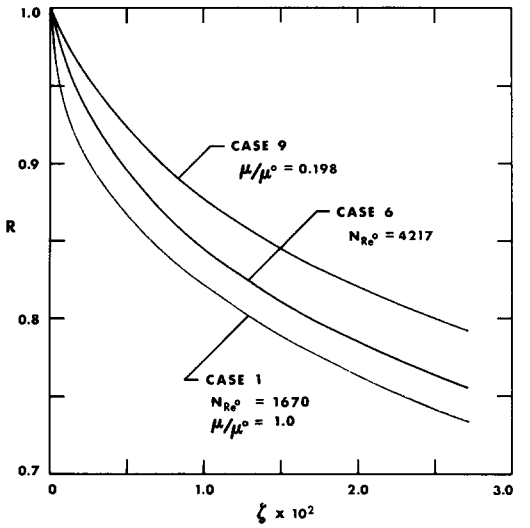

Figure 7. Effects of N_{Re}° and μ/μ° on jet radius for $N_j = 128.5$, $N_{We} = 5.4$, $N_{Re} = 835$.

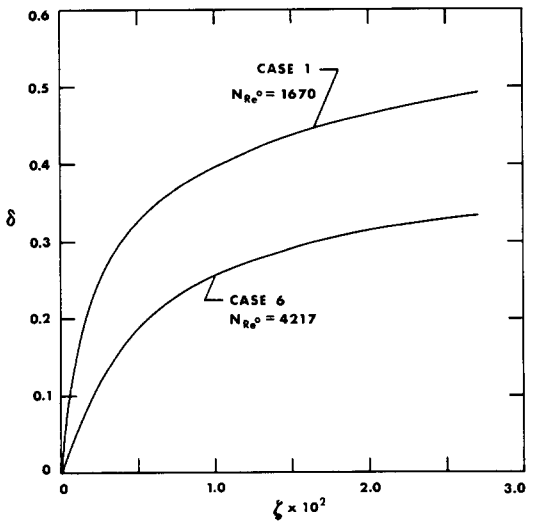

Figure 8. Effect of N_{Re}° on boundary layer thickness for $N_j = 128.5$, $N_{We} = 5.4$, $N_{Re} = 835$, μ/μ° = 1.0.

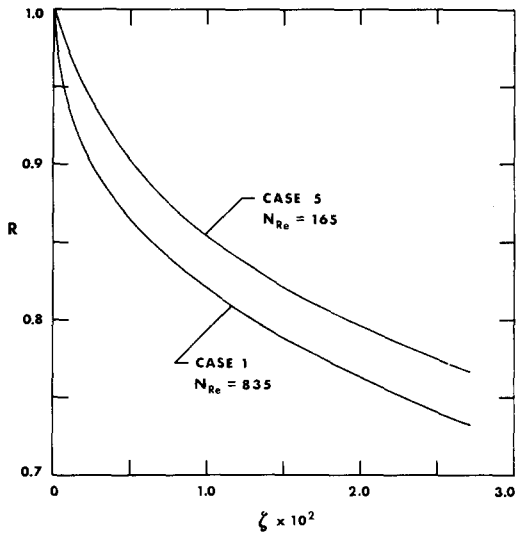

Figure 9. Effect of N_{Re} on jet radius for $N_j = 128.5$, $N_{We} = 5.4$, $N_{Re^\circ} = 1670$, $\mu/\mu^\circ = 1.0$.

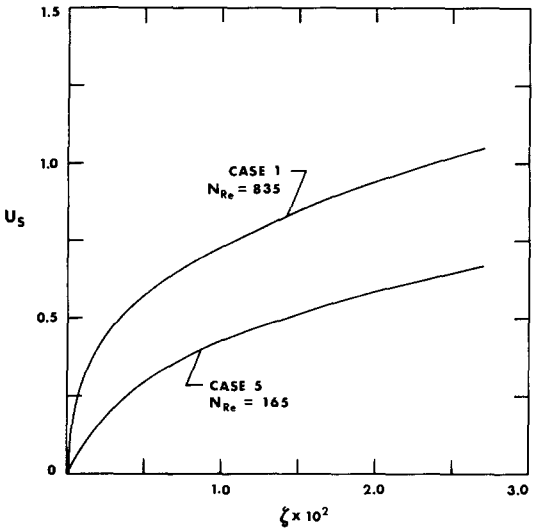

Figure 10. Effect of N_{Re} on jet surface velocity for $N_j = 128.5$, $N_{We} = 5.4$, $N_{Re^\circ} = 1670$, $\mu/\mu^\circ = 1.0$.

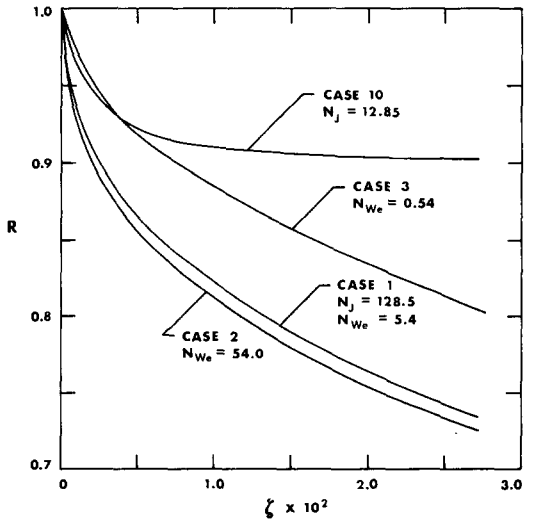

Figure 11. Effects of N_j and N_{We} on jet radius for $N_{Re} = 835$, $N_{Re^\circ} = 1670$, $\mu/\mu^\circ = 1.0$.

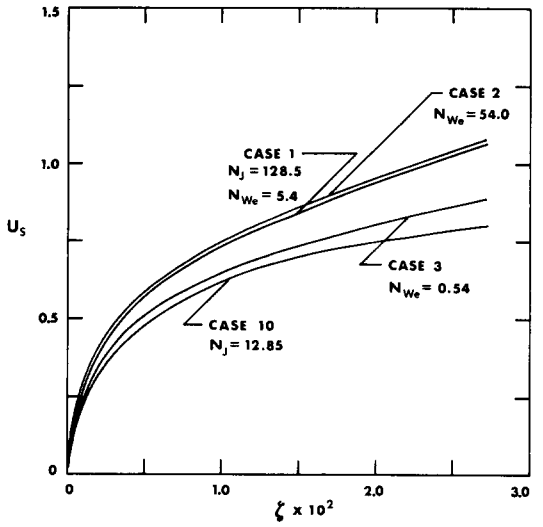

Figure 12. Effects of N_j and N_{We} on jet surface velocity for $N_{Re} = 835$, $N_{Re'} = 1670$, $\mu/\mu^\circ = 1.0$.

jet momentum resulting from a force acting in the same direction as the jet motion will increase jet contraction, while any force which opposes jet motion will reduce jet contraction. Note that jet contraction beyond $R = 0.866$ is possible when the net force acts in the direction of jet motion. Changes in jet velocity will accompany any change in jet radius since continuity must be satisfied.

The interaction of relaxation effects and jet momentum changes can produce three different types of flow behavior. Figure 2 shows the axial center-line velocity as a function of axial distance for systems 1, 3 and 10. In all three systems the interfacial velocity increases with distance downstream because of profile relaxation. In system 1 the large increase in jet momentum resulting from the upward buoyant force causes the center-line velocity to increase with distance downstream even in the region near the nozzle where profile relaxation is largest. The radial component of the dispersed phase velocity is everywhere negative. The opposite behavior is seen for system 10 where the buoyant force is small. There is a continuous decrease in center-line velocity, and the radial velocity is everywhere positive. System 3 shows intermediate behavior, with the center-line velocity decreasing initially due to jet relaxation and then increasing due to buoyancy effects.

Viscous effects

The effect of incorporating the continuous phase viscosity into the analysis is shown in figures 3–5. Figures 3 and 4 show the interfacial velocity U_s and jet radius as a function of axial distance from the nozzle for case 1, using both the present analysis and the inviscid analysis of Duda and Vrentas. Figure 5 compares the axial velocity distributions predicted by the two analysis for case 1 at the axial location $\zeta = 0.027$, which is 11.2 diameters downstream from the nozzle exit. It can be seen that the continuous phase viscosity decreases the interfacial velocity and increases the jet radius. The calculated 50% decrease in interfacial velocity and 10% increase in jet radius at $\zeta = 0.027$ illustrate the importance of the continuous phase viscosity.

The viscosity gives rise to an interfacial shear force which opposes jet motion, reducing the downstream jet momentum, and which also prevents the jet from fully relaxing to a plug flow velocity distribution. The combination of reduced jet momentum and decreased jet relaxation is responsible for the decreases in jet contraction and interfacial velocity seen in figures 3–5. The inviscid analysis of Duda and Vrentas thus provides a lower limit for jet radius.

Also shown in figure 4 is the jet radius predicted by [24] which neglects both viscous forces and jet relaxation. Equation [24] underestimates jet contraction in the region near the nozzle

where relaxation is significant and overestimates the contraction downstream where viscous forces are important. Because of the compensating nature of these errors, it is possible for [24] to give a reasonable prediction of jet radius over a portion of the flow field.

Three dimensionless parameters must be specified to characterize the effect of viscosity on jet behavior. The effects of the viscosity ratio μ/μ° and the continuous phase Reynolds number N_{Re° on the jet interfacial velocity and radius are shown in figures 6 and 7. For a given dispersed phase liquid the jet radius increases and the interfacial velocity decreases as μ° or N_{Re° increases. Increasing μ° increases the interfacial shear relative to the initial jet momentum and also reduces jet relaxation. Similar effects are associated with increasing N_{Re° because of the decreasing thickness of the continuous phase boundary layer. A comparison of the dimensionless boundary layer thicknesses for continuous phase Reynolds numbers of 1670 and 4217 is shown in figure 8.

The third dimensionless parameter characterizing viscous effects is the dispersed phase Reynolds number N_{Re}. For an inviscid continuous phase the jet radius dependence on the axial position coordinate ζ is independent of N_{Re}. Figure 9 shows that for a viscous continuous phase an increase in the jet Reynolds number decreases the jet radius at a given ζ; accompanying this decrease is a corresponding increase in interfacial velocity, as shown in figure 10.

Figures 6–10 illustrate the important role played by the three dimensionless parameters μ/μ°, N_{Re° and N_{Re} in characterizing the effect of the continuous phase on jet behavior.

Buoyancy and interfacial tension effects

Figure 11 shows the effects of buoyant and interfacial tension forces on the calculated jet radius. An increase in buoyancy, characterized by an increase in N_j, increases jet momentum and hence increases jet contraction. Similarly a decrease in the interfacial tension force, characterized by an increase in N_{We}, will increase contraction. An increase in surface velocity is associated with the increased jet contraction, as seen in figure 12. The curves for $N_j = 12.85$ show that a jet may contract to essentially its final diameter long before the velocity profile has relaxed completely. These results are consistent with those obtained by Duda and Vrentas for an inviscid continuous phase.

Figures 11 and 12 show that the significance of each force depends on its magnitude relative to the total force acting on the jet. For example, the increase in jet radius associated with a 10-fold decrease in N_{We} from 5.4 to 0.54 is much greater than that associated with a ten-fold decrease in N_{We} from 54.0 to 5.4 because the interfacial tension force becomes increasingly significant as N_{We} approaches zero.

COMPARISON OF NUMERICAL RESULTS WITH EXPERIMENTAL DATA

Experimental jet radii were measured to test the analysis. The continuous phase was contained in a tank 0.762 m high having a 0.305 m square cross section. The dispersed phase issued vertically from a 0.61 m long nozzle made of precision bore glass tubing. Nozzle diameters of 0.168, 0.251 and 0.427 cm were used, so the minimum nozzle length to diameter ratio was 143, sufficient to assure a fully developed parabolic velocity profile at the nozzle tip. Each tip was surrounded by a 10.16 cm diameter circular glass disc to approximate the continuous phase initial conditions assumed in the analysis, namely $U^\circ = V^\circ$ at $\zeta = 0$ for all $r \geq R$.

Jet radii were measured from 35 mm still photograph negatives in the region near the nozzle where disturbances on the jet surface were not visible. Each experimental radius represents the average of measurements obtained from four photographs. The average deviation of measurements from the mean was $\pm 3.5\%$.

A series of ten experiments was conducted using either benzene or heptane as the jet phase and water as the continuous phase. The systems were mutually saturated to eliminate mass transfer effects. The following ranges of parameters were investigated: N_j, 8.5–580.7; N_{We}, 2.1–19.6; μ/μ°, 0.48–0.78; N_{Re°, 714–1651; N_{Re}, 802–1855. All systems satisfied the restrictions $N_{Re^\circ} > 100$ and $N_{Re} > 200$ required to justify the order of magnitude approximations made in the

theoretical analysis, as well as the restriction $2/RN_{We} \gg [4(1-\mu^\circ/\mu)\partial U/\partial\xi]/N_{Re}$ needed to simplify [18].

The maximum deviation between measured and theoretical jet radii was 4.7%, and in eight of the ten experiments the maximum deviation was less than 3.5%. Since the experimental radii have an uncertainty of ±3.5%, the deviations are generally within the range of experimental accuracy, thus confirming the essential features of the analysis.

The results shown in figure 13 for three benzene jets injected into water are representative of the agreement found between theory and experiment. Although the agreement is within experimental accuracy for each jet, the data suggest a tendency for the theory to overestimate jet contraction in the region near the nozzle. The data also suggest that in the region far downstream from the nozzle the theory becomes less satisfactory as the viscous forces become increasingly significant.

In the region near the nozzle two factors are likely to cause theoretical inaccuracy. First, the boundary layer assumptions used in simplifying the continuous phase equations may not be valid close to the nozzle. In particular, neglect of the radial pressure gradient may not be a good approximation. Second, the assumed velocity distribution given by [28] may be inadequate. Velocity profile relaxation plays a significant role in determining jet contraction near the nozzle. It has already been pointed out that the distribution is unsatisfactory for an inviscid continuous phase, predicting instantaneous relaxation and thereby overestimating the initial rate of jet contraction.

In the region downstream from the nozzle prediction of the viscous force is the most likely source of error, not only because the error increases as the viscous force becomes increasingly significant but also because the major assumptions in the analysis have their largest effect on the interfacial shear. In particular the use of an integral analysis in each phase requires the assumptions of equations for the velocity distributions which are unlikely to represent the actual profiles accurately.

Since interfacial shear is affected by the continuous phase boundary layer thickness, a critical evaluation of the boundary layer analysis would be useful. This is not possible, because previous analyses have been restricted to continuous solid cylindrical surfaces where the cylinder radius

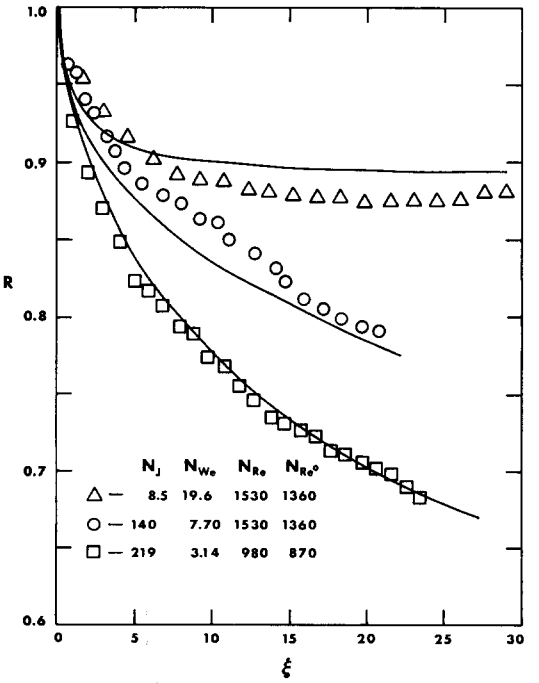

Figure 13. Comparison of experimental and theoretical jet radii.

and interfacial velocity were constant. However, if it is assumed that these analyses can be applied locally to a tapering jet with varying interfacial velocity, the boundary layer thickness predicted by the present analysis is intermediate between the values predicted by Sakiadis (1961) and by Vasudevan & Middleman (1970). Although the continuous phase Reynolds numbers are somewhat lower than those normally associated with boundary layer flows, the numerical results indicate that the boundary layer assumptions are valid except near the nozzle.

Experimental velocity distributions would provide a more rigorous test of the theory, but such data are not presently available.

CONCLUSIONS

The dimensionless continuity and momentum equations describing the flow behavior of a laminar liquid jet injected into a second immiscible liquid are complicated by the need to consider the viscosity of the continuous phase. While two dimensionless groups, a buoyancy parameter and an interfacial tension parameter, completely characterize jet behavior in an inviscid medium, three additional dimensionless groups are needed when the external fluid viscosity is not negligible.

To investigate the importance of the continuous phase on jet behavior, an approximate solution is obtained. The numerical results show that a finite continuous phase viscosity will increase the jet radius in comparison to its thickness in an inviscid fluid. All three dimensionless groups which are needed to characterize the viscous effects, namely the viscosity ratio of the two phases and the Reynolds numbers of the two phases, can significantly affect both the jet radius and velocity distribution. Specifically, the jet radius will increase with an increase in the ratio of continuous to dispersed phase viscosity, an increase in the continuous phase Reynolds number, or a decrease in the jet Reynolds number.

Experimental measurements of jet radius confirm the essential features of the analysis.

REFERENCES

ADDISON, C. C. & ELLIOTT, T. A. 1949 A new contracting liquid-jet technique for the study of soluble films at small surface ages. *J. Chem. Soc.* 2789–2805.

ADDISON, C. C. & ELLIOTT, T. A. 1950 The application of the contracting liquid-jet technique to the measurement of tensions at liquid-liquid interfaces. *J. Chem. Soc.* 3090–3096.

BROWN, K. M. & SAMUEL, D. C. 1967 The solution of simultaneous non-linear equations. Proceedings 22nd National Meeting A.C.M. 111–116.

DUDA, J. L. & VRENTAS, J. S. 1967 Fluid mechanics of laminar liquid jets. *Chem. Engng Sci.* **22**, 855–869.

GARNER, F. H., MINA, P. & JENSON, V. G. 1959 Surface aging at liquid–liquid interfaces. *Trans. Faraday Soc.* **55**, 1607–1630.

MEISTER, B. J. & SCHEELE, G. F. 1969a Prediction of jet length in immiscible liquid systems. *A.I.Ch.E. J.* **15**, 689–699.

MEISTER, B. J. & SCHEELE, G. F. 1969b Drop formation from cylindrical jets in immiscible liquid systems. *A.I.Ch.E. J.* **15**, 700–706.

SAKIADIS, B. C. 1961 Boundary-layer behavior on continuous solid surfaces. *A.I.Ch.E.J.* **7**, 26–28.

SHIFFLER, D. A. 1965 Investigation of liquid-liquid jets and droplets formed therefrom. Ph.D. Thesis, Cornell University.

VANDEGRIFT, A. E. 1963 Liquid–liquid interfacial tension measurements with an oscillating jet. Ph.D. Thesis, University of California, Berkeley.

VASUDEVAN, G. & MIDDLEMAN, S. 1970 Momentum, heat and mass transfer to a continuous cylindrical surface in axial motion. *A.I.Ch.E. J.* **16**, 614–619.

YU, H. 1971 Laminar jet contraction and velocity distribution in immiscible Newtonian liquid–liquid systems. Ph.D. Thesis, Cornell University.

Résumé—On analyse le comportement d'un jet d'un liquide newtonien, injecté verticalement dans un liquide newtonien non miscible.

On utilise des approximations du type approximations de la couche limite pour simplifier les équations générales, et on obtient une solution numérique approchée du type à intégrale de quantité de mouvement. Cette solution prédit le profil de vitesse dans les deux phases et le rayon du jet. On montre quelles sont les influences sur le comportement du jet des cinq nombres adimensionnels nécessaires pour caractériser les forces de gravité, de tension superficielle et de viscosité. On démontre en particulier l'importance de la viscosité de la phase continue. Des mesures expérimentales de rayon de jet confirment les traits essentiels de l'analyse et illustrent les insuffisances de la solution approchée.

Auszug——Das Stroemungsverhalten eines vertikal in eine nicht mischbare Phase Newtonscher Fluessigkeit eingespritzten Strahles Newtonscher Fluessigkeit wird analysiert. Durch Grenzschichtannaeherungen werden die allgemeinen Gleichungen vereinfacht, und es wird eine angenaeherte numerische Loesung in der Form eines Integrals der Bewegungsgroesse erhalten. Diese Loesung erhibt eine Voraussage fuer die Geschwindigkeitsverteilung in beiden Phasen, und fuer den Strahlradius. Fuenf dimensionslose Kennzahlen sind notwendig, um die Schwere-, Oberflaechen-, und Zaehigkeitskraefte zu kennzeichnen. Ihr Einfluss auf das Strahlverhalten wird aufgezeigt, mit besonderem Hinweis auf die Wichtigkeit der Zaehigkeit der kontinuierlichen Phase. Experimentelle Messungen des Strahlradius bestaetigen die Ergebnisse der Analyse in den wesentlichen Zuegen, und illustrieren die Grenzen der Angenaeherten Loesung.

Резюме—Аыализируется поведение потока струи некоторой ньютонианской жид кости впрыскиваемой вертикально в нерастворимую в ней ньютонианскую жидкую фазу. В целях упрощения уравнений общего вида используются приближения типа поверхностного слоя. Чем получено численное решение приближенного представление интеграла момента количества движения. Такое решение предсказывает распределение скоростей в каждой из фаз и радиус струи. Показано влияние на поведение струи пяти безразмерных групп, необходимых для характеристики сил тяжести, поверхностного натяжения и вязкости. В частности показана важность непрерывности фазовой вязкости. Экспериментальные измерения подтверждают в общих чертах указанный анализ и иллюстрируют недостатки приближенного решения.